CHAPTER 3

The IDE sensor and its design

Contents

Chapter 3: The IDE sensor and its design

3.1 Introduction

The chapter 2 presents a brief review on sensors with the advantages of IDE based capasitive sensor. In this chapter, an introduction to interdigitated electrodes (IDE) sensor, its model and the design of its geometric parameters have been elucidated for specific application in slow bitterness assessment. The capacitive sensor based on IDE structure is proposed for the research work and the capacitance model of the same has been explained.

One of the most widely deployed periodic electrode configurations is an interdigitated electrodes. The term "interdigitated," opted for use throughout this work, refers to a periodic pattern of parallel in-plane electrodes arranged in the shape of digits or fingers as shown in Fig. 3.1a. The terms "interdigital" and "combed" are frequently used in place of their equivalents, "periodic," "microstrip," "comb," and "grating". We have used the planar interdigitated structure in our work as a capacitive sensor which exhibits a large number of applications due to its quick response, miniature size, less fabrication cost and having no harmful radiation [1]. The planar interdigitated sensor has access to material from a single side of the substrate which is advantageous in comparison to double-side access to the material [2]. As IDE capacitive sensors do not consume static power, it has a wide range of applications [3]. The IDEs can incorporate sensitive material over its surface that can monitor the concentration of analyte upon its adsorption when the permittivity of the same changes.

This IDE pattern is used to increase the capacitance connected to the electric fields that permeate the material sample or sensitive coating. The material's dielectric characteristics, as well as the electrode and material shape, affect the capacitance between the two electrodes. Since changes in a material's physical, chemical, or structural properties often result in changes in its dielectric properties, dielectrometry studies provide an efficient method for the non-destructive evaluation of important parameters indirectly. A gradual change from a parallel-plate capacitor to a fringing field capacitor is depicted in Fig. 3.1b. A fringing electric field is created when the electrodes gradually widen up and the electric field is spread out across a wider area. The fringing electric field between the excitation and sensing electrodes becomes dominant as the pattern of these electrodes is transformed into a co-planar layout [4]. With the conversion from parallel plate to planar electrode structure, the effective active area of the sensor increases and subsequently increases the effective capacitance of the structure.

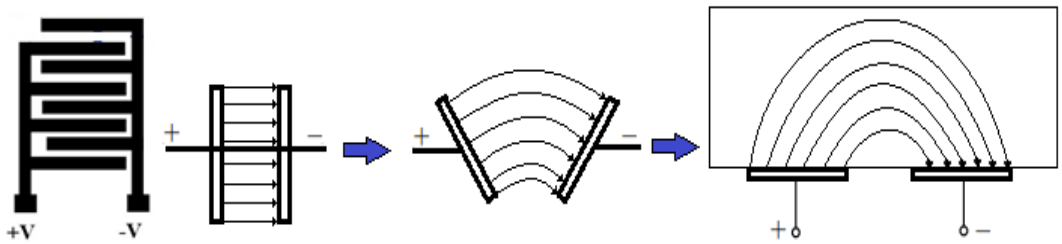

(a) (b)

Figure 3.1 (a) the IDE structure (b) Gradual transformation of parallel to planar geometry

The geometry of the sensors affects the sensitivity of the sensor and hence sensitivity can be improved by optimizing the geometry of the sensor. Hence by adjusting the sensor's surface area, the number of electrode fingers, their spacing, and the spatial wavelength, (which is the distance between the centerlines of adjacent electrodes) the strength of the output signal can be controlled. Device simulation based on the model is carried out using COMSOL multiphysics and MATLAB tool to obtain the effective design values of the device parameters such as the metallization ratio, the number of fingers, their spacing, the spatial wavelength, electrode finger width, overlapping length, etc.

3.2 Electric Fields and physical principle of sensing

The fundamental workings of a fringing field dielectrometry sensor are identical to those of a more traditional parallel-plate or coaxial cylinder dielectric sensor cell. The electrodes are given a voltage, and the impedance/ capacitance across the electrodes is then measured. The fringing field sensor, however, does not need two-sided access to the material under test (MUT), in contrast to the parallel-plate capacitor. A progressive change from a parallel-plate capacitor to a fringing field capacitor is depicted in Fig. 3.1b. In each of the three scenarios, the MUT is crossed by electric field lines, therefore the capacitance and conductance between the two electrodes are both influenced by the material's dielectric characteristics as well as by the electrode and material's geometry. To measure the dielectric characteristics of materials from one side, interdigital dielectrometry (a subset of interdigital electrode sensors) can be used [5, 6]. Typically, the stray capacitance of the leads (conductors that connect the electrodes with the electrical excitation source) is comparable to the capacitance between two coplanar strips, as shown in Fig. 3.1b. Therefore, the coplanar strip pattern may be repeated numerous

times to create an electrode configuration that is simple to measure. The distance between the centerlines of the driving and sensing fingers' centerlines, which is independent of frequency, determines how deep the fringing quasi-static electric fields above the interdigital electrodes penetrate [7, 8].

The IDE structure with its geometrical and other parameters are shown in Fig. 3.2a. The cross-sectional view of the same structure with various capacitances formed is depicted in Fig. 3.2b. Fig. 3.2c shows the unit cell of the IDE structure with the permittivity of air, dielectric material and the substrate. The measured capacitance depends on the dielectric constants of the substrate, the sensing material, and the air medium (Fig. 3.2d). When different potentials of V+ and V- are applied on the interdigitated electrodes, electric fields travel from one electrode to the other penetrating the sensing material as well as the substrate underneath the electrodes and the fringing fields traverse between the interdigitated electrodes as shown in Fig. 3.2d. The capacitances developed due to fringing fields (C_f and C_s) depend on the width of electrodes, whereas the capacitance (C_t) due to transverse electric fields can be considered as simple parallel plate capacitor depends on dielectric constant ε_m, thickness "t" of the electrode fingers and the distance between the adjacent electrodes "a" (Fig. 3.2c).

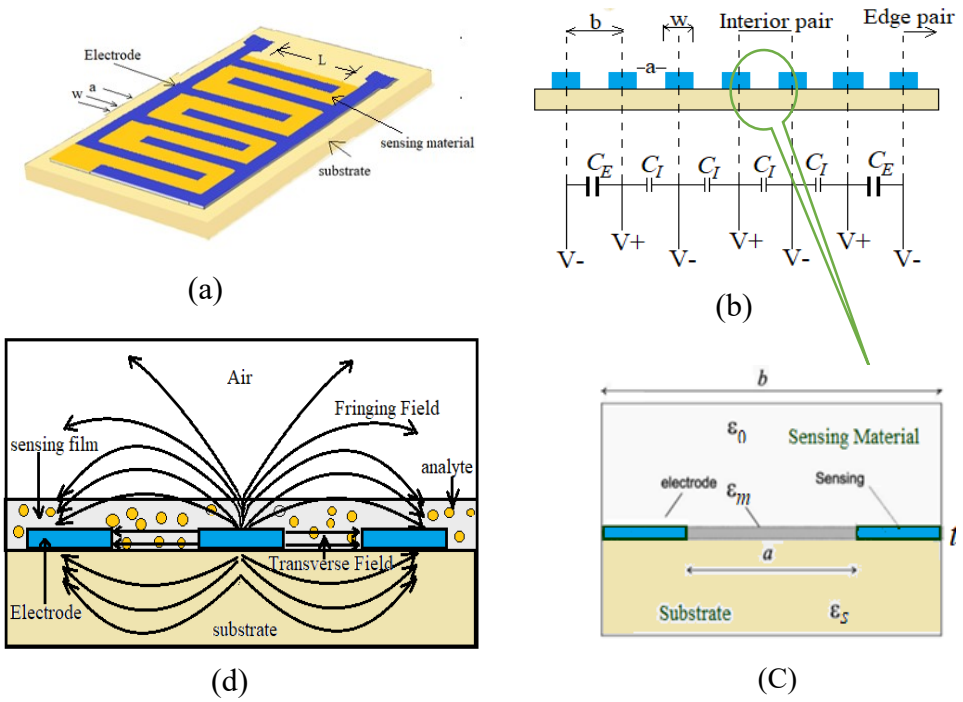

Figure 3.2: (a) Interdigitated Electrodes Structure (b) Side view of IDE showing capacitances formed (c) the unit cell of IDE with permittivities of different medium (d) fringing field and transverse field penetrating the dielectric, air and substrate medium

The distance between the centers of two adjacent electrodes is "b". The total capacitance of the IDE capacitive sensor due to both fringing fields and traverse electric fields in Fig. 3.2d is written as,

$$C_{Total} = L((N-3)C_I + 2C_E \quad (3.1)$$

where C_I is the capacitance due to the unit cell, C_E is the capacitance due to the edge electrodes (as shown in Fig. 3.2b), L is the overlapping length of the electrodes, N is the number of electrode fingers.

Conformal mapping is one of the most frequently used approaches for the calculation of the capacitance of interdigital structures, especially when the imaginary part of the complex dielectric permittivity of all materials is small enough to be neglected. Neglecting the capacitance due to the edge electrode, the total capacitance of the IDE sensor is the sum of the capacitances for the internal capacitances C_I as shown in Fig. 3.2b. Three capacitances C_t, C_s and C_f as shown in Fig 3.3 with corresponding relative permittivities of ε_m, ε_s and ε_0 will be created in this configuration. For this design, the total capacitance between the working and sensing electrodes may be calculated using Eq. (3.2) [9]

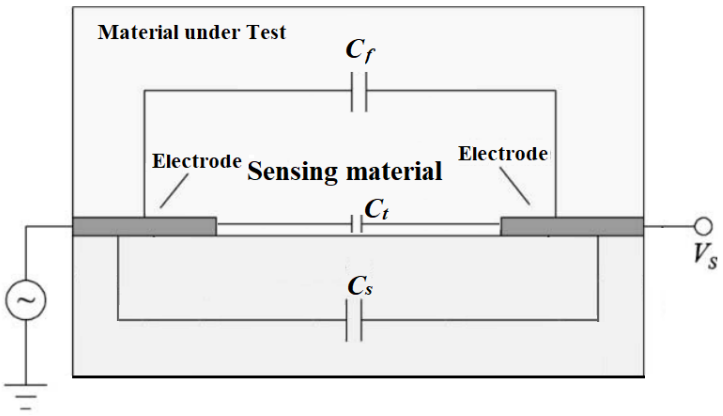

Figure 3.3: The capacitance model.

$$C_{Total} = C_t + C_s + C_f \quad (3.2)$$

Using a complete elliptic integral, of the first kind, the sum of the capacitances per unit length can be given by Eq. (3.3) [9, 10]

$$C_{Total} = L((N-3)[\varepsilon_0 \frac{\varepsilon_m+\varepsilon_s}{2} \frac{K(k^i)}{K(k)} + \varepsilon_0 \varepsilon_m \frac{t}{a}] \quad (3.3)$$

where $K(k)$ is a first-order elliptic integral, k is the elliptical modulus. t is the thickness of the electrodes

Here, k= cos (π/2*a/b) and $k^i = (1- k^2)^{1/2}$

The $K(k)$ is expressed here as

$$K(k) = \int_{t=0}^{t} \frac{dt}{[(1-t^2).(1-k^2t^2)]^{1/2}} \qquad (3.4)$$

Neglecting a very small value of the imaginary part of the complex dielectric permittivity of materials, conformal mapping approaches are used for the calculation of IDE capacitance. The capacitance per unit cell (Fig. 3.2c) is calculated by using a complete elliptic integral (of the first kind).

3.3 Simulation and Design of Parameters

As illustrated in Figure 3.1a, the IDE-based sensor is made up of two electrodes that each contains some individual fingers (digits=8 in this case) and are arranged in a comb-like shape with gaps between them. The structure of comb-like electrodes makes them simple, cost-effective, and easily adaptable to different applications without significantly affecting the design. As a result, it becomes a good candidate for applications like gas sensors and biosensors. We take the sensitive layer of cerium oxide nanoparticles for the development of a sensor for the detection of limonin in citrus fruit juices. Another sensor has been developed using magnesium silicate material over the surface of the IDE structure for both detection as well as the measurement of its reduction. Simulation has been done taking both the materials separately.

Table 3.1: Comparison of different electrode materials

Electrode material name	advantages	disadvantages
Silver	• Stability in air medium • Wide temperature range • High conductivity • Least expensive	• Not stable for long term • Tendency to migrate over the surface under high humidity
Gold	• conductivity high • reliable	• At low temperature diffusing into substrate easily • Expensive
Platinum	• stable • Wide temperature range	• High cost • Poor adhesion to substrate

The electrodes will produce an electric field when an appropriate voltage is applied to them. Regarding the sensors' sensitivity, selectivity, stability, and response time, the electrode materials of the IDEs are vital. The interaction between the sensor and electrode materials has thus been the subject of numerous research studies. Silver, gold, platinum, and palladium are the most frequently employed electrode materials. Silver is less expensive and more stable in the air than gold and platinum, although it migrates over resistor surfaces when humidity is high. Gold is famous for its high electric conductivity and reliability, but very unsuitable for solder ability and easily diffuses into

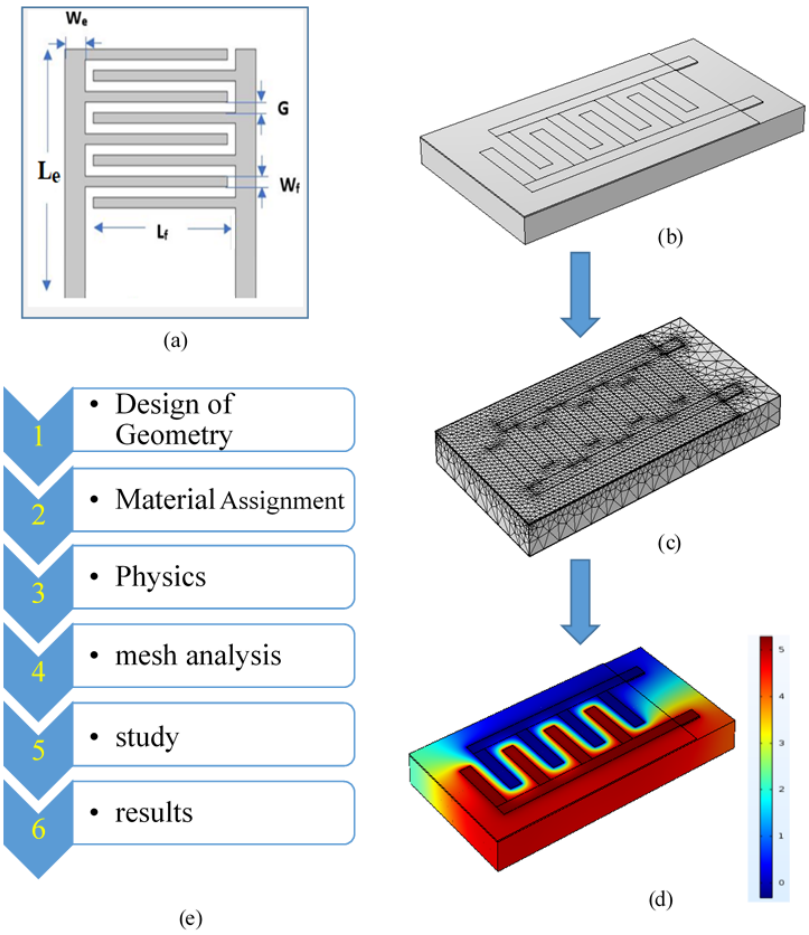

Figure 3.4: Design and optimization of IDE parameters to improve the performance of the sensor: (a) Interdigitated Electrodes Structure showing geometric parameters (b) Geometric view of comb structure designed in COMSOL Multiphysics (c) Mesh analysis of the comb structure (d) Electric field color map of IDE (e) simulation concept/ steps

a substrate like silicon at a relatively low temperature and high cost also. Platinum is also costly and has low adhesion capability to the substrate. We have used silver material for the IDE electrode for its stability, wide temperature range, high conductivity and most

importantly low-cost feature. A comparative study is listed in Table 3.1. Empirical studies on the geometric design of IDEs can be used to improve sensitivity performance. Through the use of COMSOL, the geometric parameters of digit width and gap size, number of electrodes, overlapping length, etc were examined concerning sensitivity. Fig. 3.4a shows the schematic of a capacitive sensor based on interdigitated electrodes made on a flexible paper substrate.

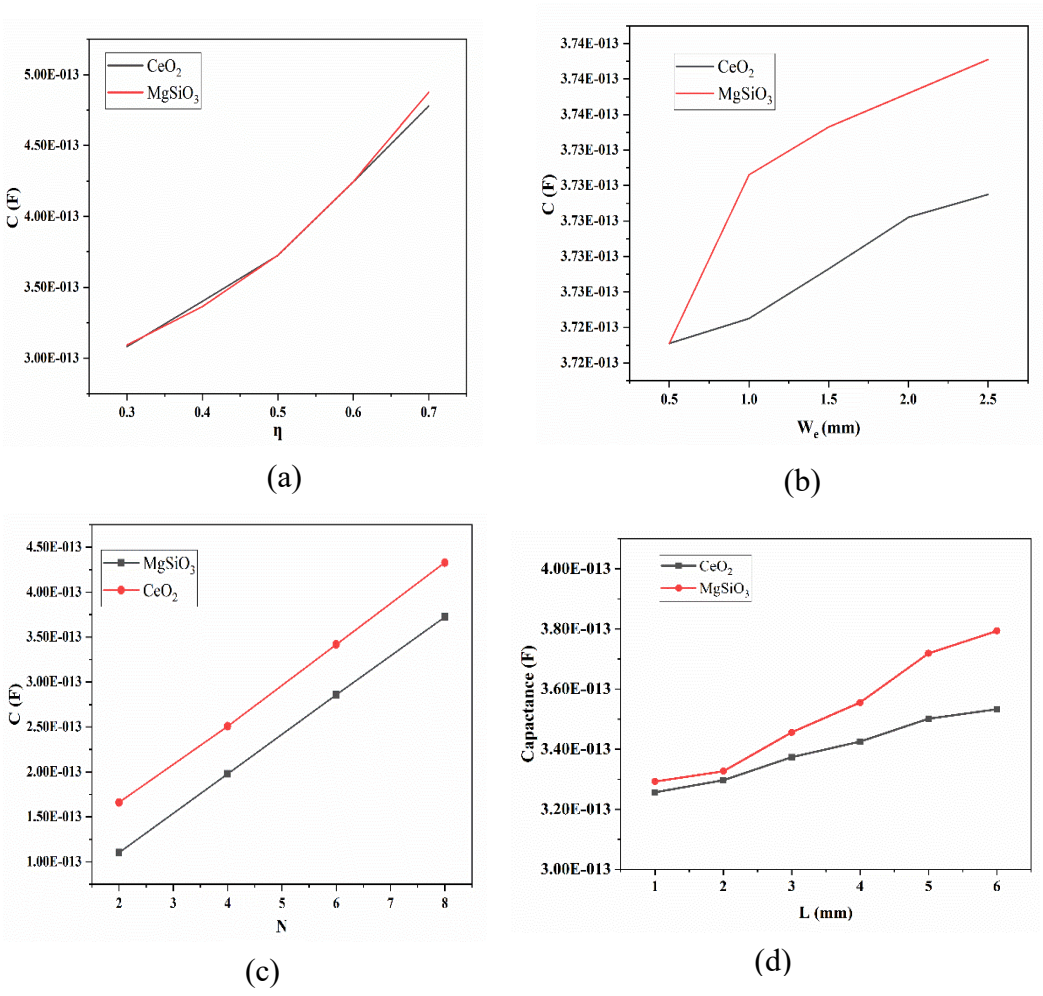

Figure 3.5: (a) IDEs capacitance vs metallization ratio for We = 1 mm, L = 5mm and and N=8 (b) capacitance vs width of the Electrodes for η=0.5, N=8 (c) Plots of Capacitance vs number of the Electrode fingers for η=0.5, N=8) (d) Change in capacitance with overlapping length of the fingers

The geometrical structure in Fig. 3.4b reveals the planner electrodes with eight numbers of fingers making the interdigitated pattern of the capacitive sensor. Here "W_f" and "G" stand for the electrode finger's width and the gap between the fingers, respectively. The

L_f, W_e and L_e represent the overlapping length of electrode fingers, the width of the electrode and the length of the electrode respectively. The ratio G/(G+ W_f) represents the metallization ratio (η). The performance of the sensor is improved by the design of the geometrical parameters of the sensor through optimization and investigation of the relationship between the parameters and the performances. Here, the IDE structure of the sensor is simulated using COMSOL Multiphysics, based on finite element analysis to obtain the effective design values of the device parameters through the meshing of IDE structure on the electrode surface (Fig. 3.4c). The electric field color mapping of the simulated IDE structure in Fig. 3.4d shows the surface potential distribution formed on the IDE-based capacitive sensing surface due to fringing and transverse field. The IDE capacitive sensor's total capacitance, C_{Total} which results from both transverse electric fields and fringing fields, is expressed as Eq. (3.1). The Fig. 3.4e shows the procedure followed for the design and simulation of IDE based capacitive structure.

For the design of the IDE pattern, the layer stack is configured along with the appropriate boundary conditions. We have simulated the device separately for both of the materials that are Cerium oxide nanoparticles and magnesium silicate to find out the capacitance change with respect to the change in its fundamental geometrical parameters such as the number of electrode fingers, metallization ratio, overlapping length and width of the electrodes. The C_{Total} increases linearly with the metallization ratio for both of the materials with an increase in the slope of the curve at a metallization ratio of 0.5 (Fig. 3.5a) indicating a high response (Table 3.2). So the metallization ratio is chosen to be 0.5 exhibiting G= W_f = 1 mm for the fabrication of the sensors. The capacitance versus the width of electrodes in Fig. 3.5b shows a linear response for CeO_2 with a slight increase in the slope at W_e=1 mm and a slight decrease in the slope at W_e= 2 mm (Table 3.3). For getting a high capacitive response we have considered W_e = 1 mm for the sensor. For $MgSiO_3$ material, the simulation results show the same trend above We= 2 mm with a slight difference in result compared to the other material. It shows a decrease in the slope below W_e =1 mm (Fig. 3.5b and Table 3.3). Fig 3.5c shows a linear increase of capacitance with the number of electrode fingers for both sensor materials (Table 3.4). From Eq. (3.1), it can be implied that the capacitance for the sensor is directly proportional to the number of fingers. For the compact design and for maintaining an appropriate exposer area of sensing materials to analytes, we have kept the number of electrode fingers at N=8. Besides this, in the design of all other parameters, the number

of fingers have considered as 8. The sensor's response to the overlapping length (L_f) of the electrode fingers was studied showing nearly linear characteristics for both sensors as shown in Fig. 3.5d and Table 3.5. As for retaining appropriate surface area for exposing the sensor material to the analyte and considering the design of other parameters we have chosen L_f to be 5mm.

Table 3.2: Capacitance for IDE vs metallization ratio for W_e=1 mm and N=8

Metallization ratio	capacitance(F), CeO_2	capacitance(F) $MgSiO_3$
0.3	3.0811E-13	3.0934E-13
0.4	3.4017E-13	3.365E-13
0.5	3.7245E-13	3.726E-13
0.6	4.245E-13	4.2456E-13
0.7	4.7798E-13	4.8768E-13

Table 3.3: Capacitance for IDE vs Width of the Electrodes for η=0.5, N=8

Width of electrodes(mm)	capacitance(F), CeO_2	capacitance(F) $MgSiO_3$
0.5	3.7231E-13	3.7231E-13
1	3.7245E-13	3.7326E-13
1.5	3.7353E-13	3.7353E-13
2	3.7302E-13	3.7372E-13
2.5	3.7310E-13	3.7391E-13

Table 3.4: Capacitance for IDE vs number of the Electrode fingers for η=0.5, N=8

Number of finger	capacitance(F), CeO_2	capacitance(F)$MgSiO_3$
2	1.6596E-13	1.1016E-13
4	2.5078E-13	1.978E-13
6	3.4177E-13	2.8571E-13
8	4.3288E-13	3.7231E-13

Table 3.5: Capacitance for IDE vs overlapping length of the Electrode fingers for η=0.5, N=8

Length in mm	capacitance(F), CeO_2	capacitance(F) $MgSiO_3$
1	3.2565E-13	3.29257E-13
2	3.297E-13	3.3267E-13
3	3.3735E-13	3.456E-13
4	3.4253E-13	3.5553E-13
5	3.5016E-13	3.719E-13
6	3.5328E-13	3.79328E-13

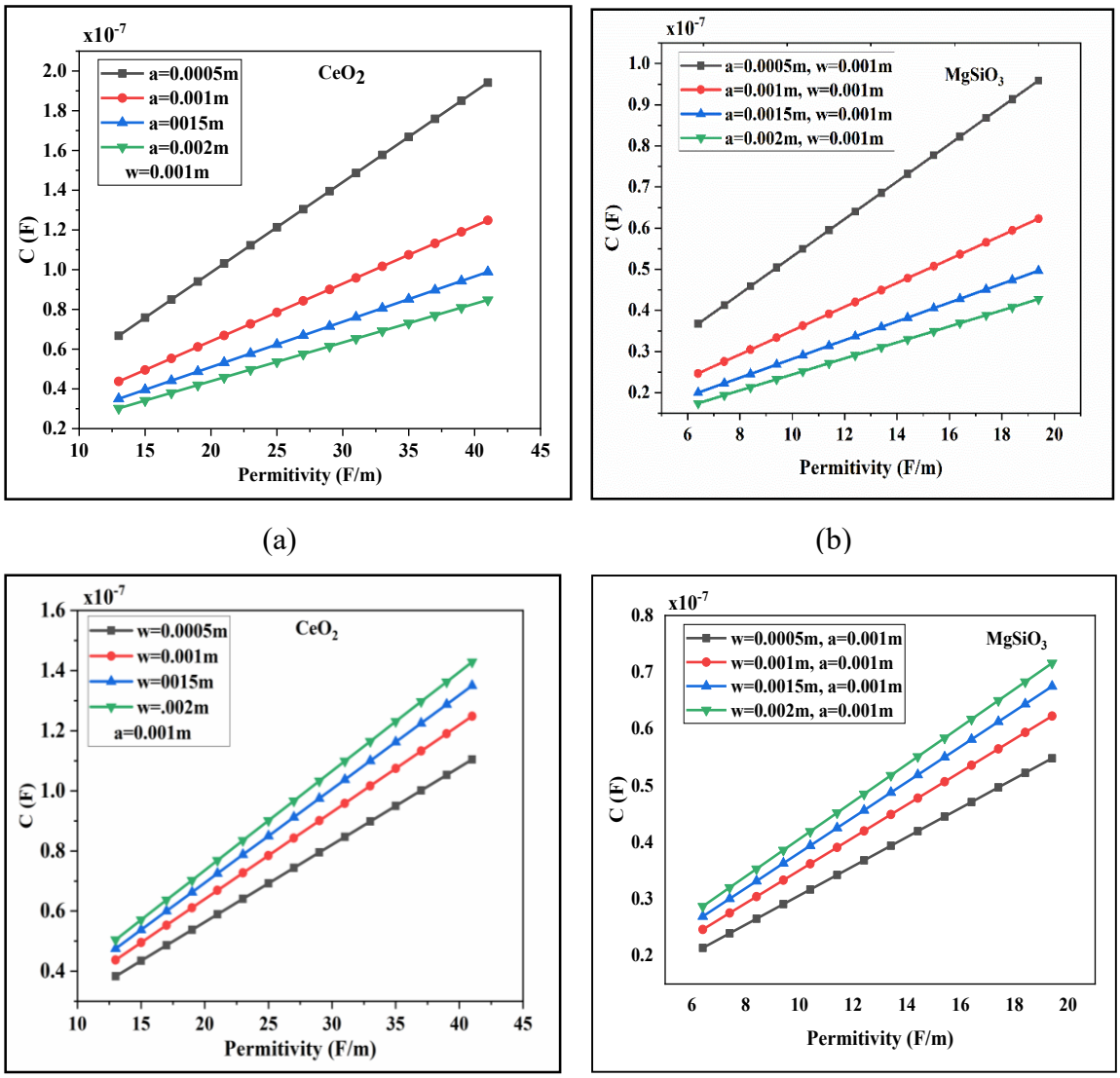

(a) (b)

(c) (d)

Figure 3.6: (a) & (b) Capacitance vs permittivity of the material for different values of "a" keeping width of the of electrodes constant (c) & (d) capacitance vs permittivity of the material for different values of "w" keeping the gap between the electrode constant

The sensor structure has been investigated using MATLAB tool to examine the way its output varies with the material's permittivity (Fig. 3.6). We have studied the capacitance versus permittivity (range approximately 10 to 40 for CeO_2 and 6.4 to 19.4 for $MgSiO_3.xH_2O$ matching with permittivity of sensing materials) for different values of width and gap of the electrode fingers and it was found that for "a" <0.001 m (a=gap between two fingers), the rate of change in capacitance for permittivity is nearly constant for both the sensors with the materials of the sensor- CeO_2 and $MgSiO_3$ (Fig. 3.6a and Fig. 3.6b). For all curves with different values of finger width, the rate of change of capacitance in response to permittivity is the same (Fig. 3.6c and Fig. 3.6d). As a result, 0.001m is the optimum value for a. The width of the fingers works out to be 0.001m so that the design value for the metallization ratio remains at 0.5 consistent with the previous optimized result for the metallization ratio.

3.4 Summary

An introduction to Interdigitated Electrodes (IDE) capacitive sensor along with its working, mathematical model based on comb fingers structure are presented. Simulation for its design parameters such as the metallization ratio, overlapping length, width of the electrodes, and finger numbers was carried out to find out the optimized design of the sensor. A construction design details of the capacitive sensor incorporating the role of the traverse and fringe capacitances of the device are presented. The capacitive response of the sensor is enhanced due to variation in the dielectric property of sensing film on exposure to analytes. The electrodes were positioned beneath a sensing film and the sensor is highly sensitive to the analyte, for which the sensitivity increases as the electrodes' spacing decreases. It was also found that the IDEs' finger length had an impact on the sensitivity. Design parameters found are η=0.5 (G=1 mm and W_f =1 mm), We = 1 mm, N =8, L_f=5 mm. Further, the studies using the MATLAB tool for capacitance versus permittivity reveal the values of the gap and width of the electrode fingers to be 0.001m making the metallization ratio equal to η=0.5 which is consistent with the results of COMSOL study. Device simulations based on the derived capacitance model provides an effective design for the development of capacitive sensor in sensing applications. We have fabricated the low-cost IDE sensor using the above design values of the design parameters for as explained in chapter 4.

Bibliography

[1] Mukhopadhyay, S. C. Sensing and instrumentation for a low cost intelligent sensing system. In *2006 SICE-ICASE International Joint Conference*, pages 1075-1080, 2006. IEEE.

[2] Abu-Abed, A. and Lindquist, R. Capacitive interdigital sensor with inhomogeneous nematic liquid crystal film. *Progress In Electromagnetics Research B,* 7:75-87, 2008.

[3] Sapsanis, C., Sivashankar, S., Omran, H., Buttner, U. and Salama, K. N. Capacitive immunosensor for C-reactive protein quantification. In *2015 IEEE 58th International Midwest Symposium on Circuits and Systems (MWSCAS)*, pages 1-4, 2015. IEEE.

[4] Hu, X. and Yang, W. Planar capacitive sensors–designs and applications. *Sensor Review*, 2010.

[5] Simpson, J. and Bidstrup, S. Modeling conductivity and viscosity changes during epoxy cure using DEA, DMA and DSC. *Polymeric Materials: Science and Engineering*:451-452, 1993.

[6] Zaretsky, M. C., Li, P. and Melcher, J. R. Estimation of thickness, complex bulk permittivity and surface conductivity using interdigital dielectrometry. *IEEE Transactions on Electrical Insulation,* 24(6):1159-1166, 1989.

[7] Sheiretov, Y. and Zahn, M. Dielectrometry measurements of moisture dynamics in oil-impregnated pressboard. *IEEE Transactions on Dielectrics and Electrical Insulation,* 2(3):329-351, 1995.

[8] Von Guggenberg, P. and Zaretsky, M. Estimation of one-dimensional complex-permittivity profiles: a feasibility study. *Journal of Electrostatics,* 34(2-3):263-277, 1995.

[9] Timmer, B., Sparreboom, W., Olthuis, W., Bergveld, P. and van den Berg, A. Planar interdigitated conductivity sensors for low electrolyte concentrations. In *SeSens 2001, Semiconductor Sensor and Actuator Technology*, pages 878-883, 2001. STW.

[10] Mamishev, A. V., Sundara-Rajan, K., Yang, F., Du, Y. and Zahn, M. Interdigital sensors and transducers. *Proceedings of the IEEE,* 92(5):808-845, 2004.